Dalton Transactions

PAPER

View Article Online
View Journal | View Issue

Cite this: *Dalton Trans.*, 2014, **43**, 5871

Chiral lanthanide complexes: coordination chemistry, spectroscopy, and catalysis†

Stacey D. Bennett,[a] Bryony A. Core,[b] Matthew P. Blake,[b] Simon J. A. Pope,[a] Philip Mountford[b] and Benjamin D. Ward*[a]

Received 13th January 2014,
Accepted 19th February 2014

DOI: 10.1039/c4dt00114a

www.rsc.org/dalton

The coordination chemistry and catalytic applications of organometallic and related lanthanide complexes bearing chiral oxazoline ligands is an area that has been largely underdeveloped, in comparison to complexes based upon lanthanide triflates for use in Lewis acid catalysis. In this article we report on the coordination chemistry of the bis(oxazolinylphenyl)amide (BOPA) ligand with lanthanide alkyl and amide co-ligands (Ln = Y, La, Pr, Nd, Sm). Their structural and spectroscopic characterisation are reported, including an assessment of their photophysical properties using luminescence spectroscopy, and are supported by density functional calculations. The application of these complexes in the hydroamination/cyclisation of aminoalkenes, and in the ring-opening polymerisation of *rac*-lactide is reported.

Introduction

The properties of the lanthanides are such that a rich and diverse range of chemistries are readily available in a number of fundamental and applied areas,[1] including a remarkable array of applications in catalysis. In addition, their unique photophysical properties provide the means with which to study the properties of their complexes by directly interrogating the metal ion.[2] The coordination chemistry of the lanthanides lacks the strong geometrical preferences seen for many of the transition metals, and therefore their coordination sphere must be controlled by the judicious selection of ligand, if highly controlled coordination environments are to be formed. Such well-defined complexes are a crucial goal for functional metal complexes, *e.g.* in catalysis research. The choice of ligand that can most efficiently provide a well-defined coordination environment must take into consideration the number and type of donor atoms, as well as the peripheral ligand architecture that will contribute to both the steric footprint of the ligand, and the relative proximity of the donor atoms within the ligand framework.

In the development of chiral metal complexes, there are few ligands that have met with greater success than oxazoline ligands, which have found widespread applications in catalysis, particularly with late transition metals.[3–7] These ligands have a number of key advantages when compared to many ligand environments: they are derived from α-amino acids, thus ensuring an ample source of chiral pool building blocks; their synthesis is facile, often being derived from nitrile or carboxylic acid derivatives, thereby providing an effectively limitless number of available ligand architectures. The chiral group adjacent to the coordinating nitrogen donor places the stereodirecting group in the most efficient position to effectively control the chiral space at the catalytically active site. The development of lanthanide catalysts bearing oxazoline ligands has steadily increased over the last 15 years, with an impressive range of applications in Lewis acid catalysis being reported.[1j] These studies often involve the coordination of oxazoline ligands to lanthanide triflates. However, the development of the corresponding organometallic and related complexes, and their associated reactions (*e.g.* polymerisation, heterofunctionalisation, *etc.*) is much less developed.[1j,8–17] The application of oxazoline ligands in lanthanide catalysis has been limited by the propensity of the lanthanides to form complexes with high coordination numbers to meet steric demands, due their inability to adopt predictable coordination geometries, whilst many of the most commonly used oxazoline ligands (*e.g.* the bis(oxazolinyl)methane "BOX" and pyridine-bisoxazoline ligands "PYBOX") have wide bite angles, and in some cases

[a]*School of Chemistry, Cardiff University, Main Building, Park Place, Cardiff CF10 3AT, UK. E-mail: WardBD@Cardiff.ac.uk*
[b]*Chemistry Research Laboratory, University of Oxford, Mansfield Road, Oxford OX1 3TA, UK. E-mail: Philip.Mountford@Chem.ox.ac.uk*

†Electronic supplementary information (ESI) available: Experimental procedures, characterising data, crystallographic data in CIF format, the molecular structure of **6b**, coordinates of all calculated structures, and catalysis data. CCDC 903609 and 980871. For ESI and crystallographic data in CIF or other electronic format see DOI: 10.1039/c4dt00114a

offer insufficient control over the lanthanide coordination geometry. In addition, oxazoline ligands have shown a tendency to undergo ring-opening in the presence of strongly basic alkyl or amide co-ligands when supported by Lewis acidic lanthanide or early transition metals.[17,18] In each case, the alkyl or amide co-ligand effectively attacks the imino carbon of the oxazoline, thereby affording an alkoxide ligand derived from the oxazoline oxygen. Such reactivity patterns highlight some of the challenges to be overcome and guarded against when undertaking such studies.

As part of our ongoing research program into the applications of polydentate oxazoline ligands with Lewis acidic metals, we have concentrated on the chiral bis(oxazolinylphenyl)amide (BOPA) ligand, which features a diphenylamide spacer between the oxazoline rings and thus a narrower bite angle than, for example, the BOX ligand. The BOPA ligand has been applied to a variety of asymmetric transformations using late transition metals, including Friedel–Crafts alkylation, hydrosilylation and the allylation of aldehydes.[17,19–23] This ligand, in its deprotonated form, is ideal to provide a lanthanide-sensitising antenna whilst encapsulating the metal within a tridentate core that offers sufficient steric demand to stabilise lanthanide alkyl and amido complexes. A report of this ligand being used to support scandium, yttrium, lutetium and thulium complexes has been recently published.[17] The authors stated that the alkyl (CH_2SiMe_3) complexes of yttrium and thulium were unstable with respect to the aforementioned insertion/ring-opening chemistry. Nevertheless, the scandium and lutetium complexes were found to be active in the polymerisation of isoprene.

Our aims are to develop the area of chiral lanthanide complexes bearing oxazoline ligands, focussing on their applications in catalysis, whilst using their photophysical properties to provide detailed insight into their structure. We have recently published a preliminary communication in which the complexes [Nd(R-BOPA){$N(SiMe_3)_2$}$_2$] were studied from both catalytic and photophysical standpoints. We demonstrated that the lanthanide emission profiles provided information relating to their structure that was unobtainable by, for example, NMR spectroscopy. This information exposed a molecular process that helps to explain the ability of the complexes to invoke stereoselectivity in catalysis.[16] In this contribution we report a detailed study of the coordination chemistry of Group 3 and lanthanide alkyl and amide complexes bearing the BOPA ligand, and probe their efficacy in the hydroamination/cyclisation of aminoalkenes and in the polymerisation of *rac*-lactide.

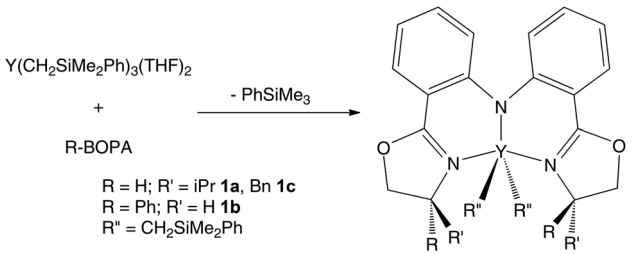

Scheme 1 Synthesis of [Y(R-BOPA)(CH_2SiMe_2Ph)$_2$].

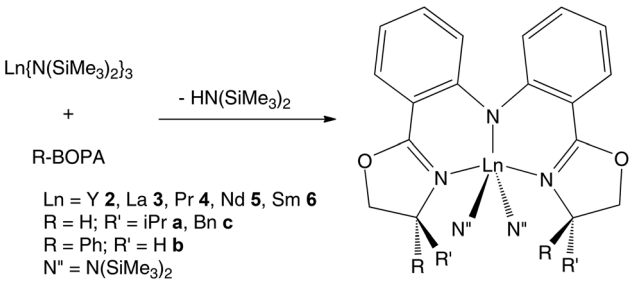

Scheme 2 Synthesis of [Ln(R-BOPA){$N(SiMe_3)_2$}$_2$].

Results and discussion

Synthesis and characterisation of lanthanide BOPA complexes

The diastereomerically pure protio ligands of R-BOPA react with the yttrium alkyl precursor [$Y(CH_2SiMe_2Ph)_3(THF)_2$] to afford the bis(alkyl) complexes [Y(R-BOPA)(CH_2SiMe_2Ph)$_2$] (R = iPr **1a**, Ph **1b**, Bn **1c**) with the concomitant elimination of phenyltrimethylsilane (Scheme 1). In contrast to the report by Zhang and Li,[17] we did not observe any oxazoline ring-opening in these complexes, which we attribute to the greater steric demand of the CH_2SiMe_2Ph, compared to the CH_2SiMe_3 group employed in their report. This difference in reactivity upon replacing a peripheral methyl group for a phenyl is unsurprising since the initial reports of using the CH_2SiMe_2Ph alkyl ligand in Group 3/lanthanide chemistry indicated that these species possess a significantly greater thermal stability when compared to the CH_2SiMe_3 congeners.[24,25] Nevertheless, in due consideration of likely side-reactions with larger lanthanide alkyl complexes, we turned our attention to the bis(trimethylsilyl)amide complexes for these metals. The BOPA protio-ligands react with the amido precursors [Ln{N($SiMe_3$)$_2$}$_3$] to afford the bis(amido) complexes [Ln(R-BOPA){$N(SiMe_3)_2$}$_2$] (Scheme 2, Ln = Y **2**, La **3**, Pr **4**, Nd **5**, Sm **6**). In the case of yttrium, the BOPA ligands failed to coordinate unless a slightly elevated temperature (40 °C) was used, whereupon complex formation was complete in 48 hours. This is presumably due to the combination of a relatively bulky amide ligand and the smaller ionic radius of yttrium, since the larger metals La, Pr, Nd, and Sm did not require any heating, the reactions being complete on leaving at ambient temperature overnight. Attempts to prepare the analogous dimethyl (achiral) BOPA derivative were unsuccessful.

The structures of [Ln(Ph-BOPA){$N(SiMe_3)_2$}$_2$] (Ln = Nd **5b** and Sm **6b**) were confirmed using X-ray crystallography. The structures are isomorphous; the molecular structure of the neodymium congener is shown in Fig. 1, and selected bond lengths and angles for both structures are in Table 1. Full refinement details for both structures are provided in the ESI.†

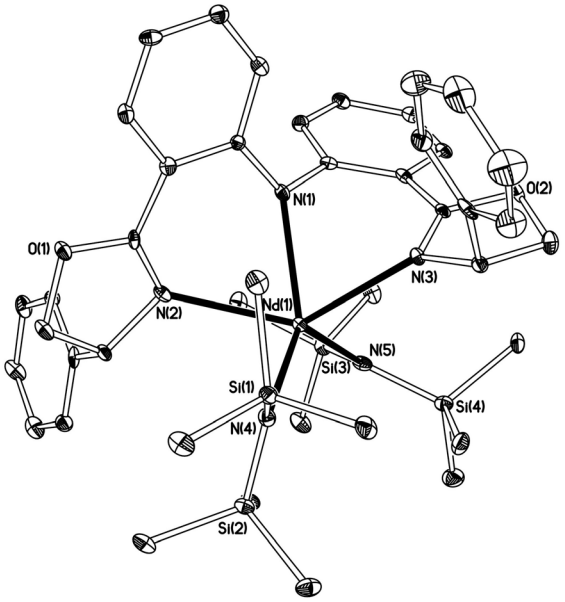

Fig. 1 Molecular structure of [Nd(Ph-BOPA){N(SiMe$_3$)$_2$}$_2$] **5b**. H atoms omitted for clarity, and displacement ellipsoids drawn at 35% probability.

Table 1 Selected bond lengths (Å) and angles (°) for [Ln(Ph-BOPA)-{N(SiMe$_3$)$_2$}$_2$] (Ln = Nd **5b** and Sm **6b**)

	5b (Ln = Nd)	**6b** (Ln = Sm)
Ln–N(1)	2.415(3)	2.3874(18)
Ln–N(2)	2.535(4)	2.5286(19)
Ln–N(3)	2.551(3)	2.5062(18)
Ln–N(4)	2.360(3)	2.3007(19)
Ln–N(5)	2.332(3)	2.3430(19)
N(1)–Ln–N(2)	70.12(11)	70.70(6)
N(1)–Ln–N(3)	69.97(11)	71.07(6)
N(1)–Ln–N(4)	132.39(11)	109.92(7)
N(1)–Ln–N(5)	110.03(11)	134.10(6)
N(2)–Ln–N(3)	131.50(11)	133.20(6)
N(4)–Ln–N(5)	117.50(12)	115.92(6)

The lanthanide ions adopt highly distorted trigonal bipyramidal geometries, with the oxazoline nitrogens occupying the axial positions, and the three amide ligands lying in the equatorial plane (sum of N_{amide}–Ln–N_{amide} angles = 359.92(34)° for **5b** and 359.94(19)° for **6b**). The BOPA ligand therefore occupies an approximate *mer* coordination motif, but with $N_{oxazoline}$–Ln–$N_{oxazoline}$ bond angles of 131.50(11)° and 133.20(6)° for **5b** and **6b** respectively, which deviate significantly from the ideal 180° and arise from a combination of the restrictions imposed by the relatively rigid BOPA ligand backbone and steric repulsion from the bulky N(SiMe$_3$)$_2$ co-ligands. The BOPA ligand adopts a conformation in which the phenyl rings of the ligand backbone are not coplanar, giving a helical twist to the diphenylamido backbone. This could, in principle, afford each complex in two diastereomeric forms, by virtue of the combination of helical chirality and the oxazoline chirality. These two forms were found to pertain in solution and were identified spectroscopically (*vide infra*). All bond distances were within the expected range based upon related examples in the Cambridge Structural Database.[26]

The NMR spectroscopic data of [Y(R-BOPA)(CH$_2$SiMe$_2$Ph)$_2$] **1a–c** are consistent with the overall C_2-symmetry depicted in Scheme 1. The ^{1}H and ^{13}C{^{1}H} NMR spectra possess signals attributed to the R-BOPA ligand which are shifted from those of the uncoordinated protio-ligand. Signals attributed to the methyl groups of the alkyl ligands are observed as two distinct singlets in the expected region close to 0 ppm; the metal-bound methylene protons were observed as diastereotopic doublets of doublets between 0 and −1.2 ppm, with associated $^2J_{YH}$ values of 2.7 Hz, comparable to previously reported examples.[10,27] The most notable difference in the spectra of complexes **1a–c** is that the isopropyl and phenyl derivatives **1a** and **1b** exist in two isomeric forms in a 1 : 0.2 and 1 : 0.6 ratio respectively, whilst the spectra of the benzyl derivative **1c** only possess a single set of resonances. 2D NMR experiments confirmed an identical connectivity in both species, and spin saturation transfer experiments indicated that the two species were interconverting. We therefore assign the two species as those containing different senses of helical twist in the diphenylamido backbone, affording two diastereomers. The structure of the isomers, and their relative energies, were probed using DFT calculations and are discussed below, although we note that the experimental ΔG_{293} values for these equilibria are 0.9 and 0.3 kcal mol^{-1} for **1a** and **1b** respectively, which are at the limits of computational accuracy.

The NMR spectra of the corresponding amido complexes **2–6** are likewise consistent with C_2 symmetric species. The spectra of the yttrium and lanthanum complexes **2** and **3** are similar to the spectra of **1**. As expected, the signals in the ^{1}H NMR spectra of the paramagnetic praseodymium, neodymium, and samarium complexes are broadened, with a reduction in fine structure, and are found over a larger chemical shift range, *i.e.* +35 to −70 (Pr), +20 to −40 (Nd), and +10 to −2 (Sm) ppm. For the yttrium complexes **2a–c**, a second (minor) component was observed in all spectra, which we again attribute to isomers with the opposite helical sense at the ligand backbone. No such species were observed in the spectra of the larger metals, even at when the spectra were recorded at reduced temperature (−80 °C).

The complexes were all employed in the hydroamination/cyclisation of aminoalkenes (*vide infra*). In order to use spectroscopic analysis as a means of providing insight into the effect of the ligand structure on the catalytic performance, complexes were prepared and characterised that are representative of the resting state of the catalyst during this reaction. Hydroamination/cyclisation catalysis proceeds by the protonation of an alkyl or amido co-ligand by the aminoalkene substrate, affording a tethered amidoalkene.[15a–d] This species will spontaneously undergo insertion into the M–N bond, thereby affording the cyclic product. Isolating the intermediate, prior to alkene insertion, presents a challenge owing to the intramolecular nature of the reaction, and we therefore prepared a *pseudo*-substrate, in which the alkene of the substrate was exchanged for a saturated counterpart. Such a species, when

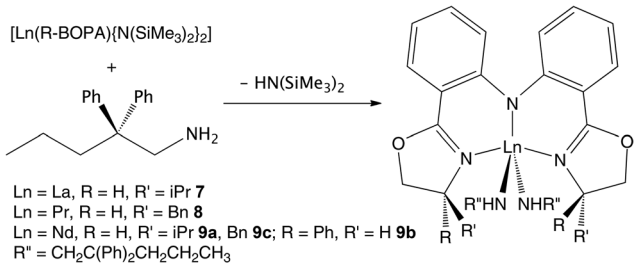

Ln = La, R = H, R' = iPr **7**
Ln = Pr, R = H, R' = Bn **8**
Ln = Nd, R = H, R' = iPr **9a**, Bn **9c**; R = Ph, R' = H **9b**
R" = $CH_2C(Ph)_2CH_2CH_2CH_3$

Scheme 3 Synthesis of $[Ln(R\text{-}BOPA)(NHCH_2CPh_2C_3H_5)_2]$.

coordinated to a metal, cannot undergo cyclisation and represents the closest possible analogue to the postulated catalyst resting state.

The complexes $[La(iPr\text{-}BOPA)(NHCH_2CPh_2C_3H_5)_2]$ **7**, $[Pr(Bn\text{-}BOPA)(NHCH_2CPh_2C_3H_5)_2]$ **8** and $[Nd(R\text{-}BOPA)(NHCH_2CPh_2C_3H_5)_2]$ (R = iPr **9a**, Ph **9b**, Bn **9c**) were prepared by the addition of 2,2′-diphenyl-aminopentane to the corresponding amido complexes, with the elimination of $HN(SiMe_3)_2$ (Scheme 3). The most valuable information was obtained using luminescence spectroscopy for the neodymium complexes, and therefore the complexes were prepared for all possible stereodirecting groups. Conversely, the praseodymium complexes proved less informative, with less variation of the spectral profile on alteration of the BOPA stereodirecting group, and so only one derivative was prepared, as a representative example. The lanthanum complex was prepared as a diamagnetic analogue to aid structural verification by NMR spectroscopy. The NMR spectra of complexes **7**–**9** show similar features to their precursors, with the exception of the absence of silyl signals, and the presence of signals corresponding to the tethered amidoalkane. Analysis of the spectra suggests the presence of only one diastereomer in each case.

Luminescence measurements

Upon coordination of the R-BOPA ligands to the lanthanide alkyls and amides it was noted that solutions of the complexes fluoresced under ambient light excitation. Our earlier studies revealed that visible light irradiation (λ_{ex} = 485 nm) stimulated emission from the complexes (in dry toluene solution, under N_2), typically characterised by a broad, unstructured luminescence band peaking *ca.* 505 nm. Time-resolved measurements were also obtained and showed that the lifetimes (all ≤5.0 ns) were subtly influenced by the ligand substituents. The emission spectra of $[La(R\text{-}BOPA)\{N(SiMe_3)_2\}_2]$ **3a–c** are displayed in Fig. 2. Additional TD-DFT calculations have been carried out for **3c**, and show that the excitation is predicted to be dominated by n→π* and π→π* transitions (Table 2), including a charge transfer (n→π*) component originating from the deprotonated/coordinated amide bridgehead. These calculations support the observations from the experimental data.

We have previously reported that the BOPA ligands successfully act as sensitising chromophores for Nd(III), inducing emission in the near-IR region consistent with the encapsulation of the ion. Photophysical studies were extended to the

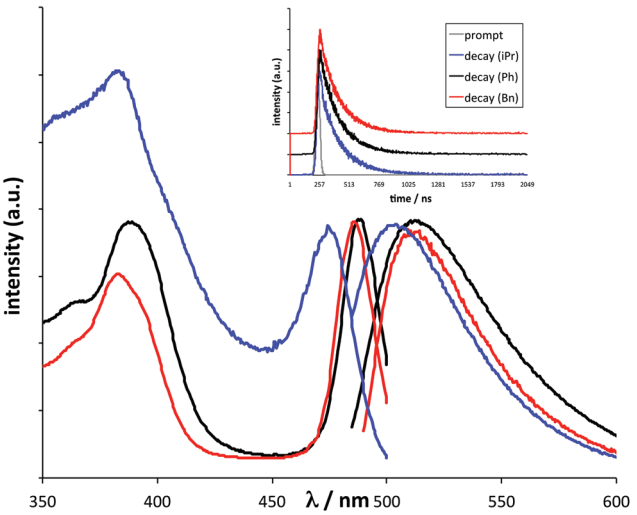

Fig. 2 Visible luminescence properties of $[La(R\text{-}BOPA)\{N(SiMe_3)_2\}_2]$ (**3a–c**): main, steady state excitation and emission spectra (λ_{ex} 485 nm) (black – Ph; red – Bn; blue – iPr). Inset, lifetime decay profiles (λ_{ex} 459 nm) of 5.0 (^{i}Pr), 4.6 (Ph) and 4.5 ns (Bn).

Table 2 Summary of TD-DFT excitation transitions for $\mathbf{3c}_{calc}$

State	Transition energy (nm)	Participating MO	Transition character
Singlet	457 (0.1699)[a]	HOMO → LUMO (0.70)[b]	n→π*[c] π→π*
Singlet	381 (0.0116)	HOMO−2 → LUMO (0.69)	n→π*[d]
Singlet	375 (0.0252)	HOMO → LUMO+1 (0.68)	n→π*[c] π→π*
Singlet	313 (0.0389)	HOMO → LUMO+3 (0.48); HOMO → LUMO+5 (0.37)	n→π*[c] π→π*
Singlet	305 (0.0196)	HOMO−3 → LUMO (0.67)	π→π*

[a] Oscillator strength. [b] Expansion coefficient. [c] BOPA amide-based. [d] $N(SiMe_3)_2$ amide-based.

lanthanide complexes containing Pr **4a–c** and Sm **6a–c**. For the Pr complexes the near-IR emission at *ca.* 1020 nm resulting from the $^1D_2 \rightarrow {}^3F_J$ (J = 3,4) transitions were extremely weak and thus uninformative. However corresponding lifetimes (Table 4) were obtained (30–47 ns) as reported for the previous examples and found to be significantly shorter than the analogous neodymium species. For the visibly emitting samarium complexes the intense residual fluorescence, which is indicative of very inefficient energy transfer, of the bridging ligand obscures the majority of the Sm(III)-centred emission bands, with only the $^4G_{5/2} \rightarrow {}^6H_{9/2}$ transition observable as a weak band at *ca.* 640 nm.

Therefore the photophysical properties of the neodymium complexes **5a–c** were the most informative, compared to the praseodymium and samarium complexes. The emission profiles for the complexes bearing the *pseudo*-hydroamination substrate $[Nd(R\text{-}BOPA)(NHCH_2CPh_2C_3H_5)_2]$ (R = iPr **9a**, Ph **9b**, Bn **9c**) were recorded in toluene (Fig. 3). In each case, the three observed near-IR transitions were attributed to $^4F_{3/2} \rightarrow {}^4I_{9/2}$, $^4F_{3/2} \rightarrow {}^4I_{11/2}$ and $^4F_{3/2} \rightarrow {}^4I_{13/2}$ transitions which are

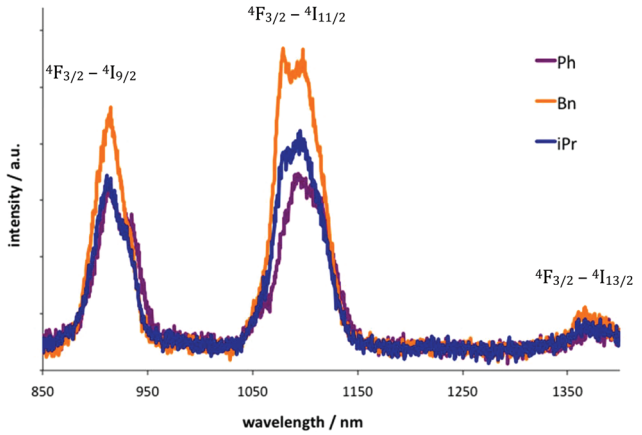

Fig. 3 Comparison of near-IR luminescence spectra (10^{-4} M, toluene, λ_{ex} 445 nm) for **9a/b/c**.

Table 3 Lifetime measurements for [Ln(R-BOPA){N(SiMe$_3$)$_2$}$_2$] (Ln = Pr **4**, Nd **5**) and related complexes (toluene, N_2, λ_{ex} = 355 nm; λ_{em} = 1010 nm for **4**, 1055 nm for **5**)

Complex	Lifetime (τ)/ns
[Pr(iPr-BOPA){N(SiMe$_3$)$_2$}$_2$] **4a**	34 (weak)
[Pr(Ph-BOPA){N(SiMe$_3$)$_2$}$_2$] **4b**	30 (weak)
[Pr(Bn-BOPA){N(SiMe$_3$)$_2$}$_2$] **4c**	47 (weak)
[Pr(Bn-BOPA)(NHCH$_2$CPh$_2$C$_3$H$_5$)$_2$] **8**	32
[Nd(iPr-BOPA){N(SiMe$_3$)$_2$}$_2$] **5a**	148, 621 (70%)
[Nd(Ph-BOPA){N(SiMe$_3$)$_2$}$_2$] **5b**	129, 677 (90%)
[Nd(Bn-BOPA){N(SiMe$_3$)$_2$}$_2$] **5c**	41, 308 (80%)
[Nd(iPr-BOPA)(NHCH$_2$CPh$_2$C$_3$H$_5$)$_2$] **9a**	111, 267 (59%)
[Nd(Ph-BOPA)(NHCH$_2$CPh$_2$C$_3$H$_5$)$_2$] **9b**	71, 165 (90%)
[Nd(Bn-BOPA)(NHCH$_2$CPh$_2$C$_3$H$_5$)$_2$] **9c**	41, 182 (93%)
[Nd(Bn-BOPA){N(SiMe$_3$)$_2$}$_2$] **5c**/catalysis[a]	81, 252 (85%)

[a] After cyclisation of 2,2-diphenyl-aminopentene.

commonly observed for Nd(III).[28] The corresponding lifetimes are provided in Table 3. The lifetimes of lanthanide excited states are highly sensitive to the local coordination environment,[29] and provide information relating to the relative concentration of nearby quenchers, such as C–H, N–H and O–H oscillators (*e.g.* from solvent, and/or coordinated substrates *etc.*).[30] This can provide information relating to the degree of steric protection offered by the supporting ligand; the steric demand of the supporting ligand set is largely responsible for the stability and selectivity (particularly stereoselectivity) in catalytically active complexes.

The lifetimes of **5a–c** fitted best to a bi-exponential decay, providing two distinct lifetimes for each complex and suggesting that **5a–c** exist in two different environments; these two species are therefore likely to be attributed to the two diastereomeric isomers previously alluded to for this class of complex. The implication is that even though, contrary to the yttrium complexes, the NMR data for the larger lanthanide complexes show no evidence for the presence of isomeric forms, these isomers nevertheless do exist, but are likely to be interconverting faster than the NMR timescale. The luminescence data therefore provide information about the molecular structure of these specific complexes that was not apparent from the data obtained using other spectroscopic techniques. We therefore suggest that luminescence spectroscopy can be used as a complementary technique, to expand the repertoire of spectroscopic methods used for structure elucidation in organometallic lanthanide complexes. These observations suggest that the two conformations of the BOPA ligand may render the metal centre less or more accessible to solvent molecules in the major and minor isomers respectively, depending on the sense of helical twist and the associated alterations in the ligand periphery. There was a difference in the observed proportions of the two isomers, dependent on the identity of the stereodirecting group. The phenyl complex **5b** showed the least proportion of the minor isomer (10%), followed by the benzyl (20%) and isopropyl (30%) congeners. As a first approximation, these figures can be related to the effective shielding of the reaction space offered by the stereodirecting group, *i.e.* phenyl being the most effective. This is supported by many catalysis studies, in which phenyl-substituted oxazoline complexes often give the greatest levels of stereocontrol.[3–7]

Neodymium complexes are distinctly advantageous in this context compared to praseodymium and samarium, since the emission profiles are known to be sensitive to the local coordination environment, and may vary as a function of ligand identity (donor type and symmetry) and/or conformation. Therefore the photophysical data for [Nd(R-BOPA)(NHCH$_2$CPh$_2$C$_3$H$_5$)$_2$] (R = iPr **9a**, Ph **9b**, Bn **9c**) were probed and were found to be similar to those of **5a–c**, in that the data suggest two distinct species with markedly different lifetimes. The lifetimes themselves were generally shorter than for the amide complexes **5a–c** which is consistent with the less rigid nature of the tethered *pseudo*-substrate, but in each case the major component retained the longest lifetime, as observed for **5a–c**. The relative weighting of the two components of **9a–c** were subtly altered upon changing the co-ligand, with the phenyl and benzyl being roughly equal at 90 : 10, and the isopropyl congener being close to 60 : 40; this is consistent with the relative stability of the components being dictated primarily by sterics, although the precise factors governing the relative stability of the two isomers is likely to be more complex in the presence of co-ligands that have a more flexible structure, and possess less predictable conformations in solution. Analysis of the reaction mixture containing **5c** after cyclisation of 2,2-diphenyl-aminopentene again indicated the presence of two isomers. It is noteworthy that there was a subtle alteration in the relative proportion of the isomers (85 : 15 ratio, compared with **5c** which gave an 80 : 20 ratio). This suggests that the proportion of the isomers may change at each stage of a catalytic reaction, which is unsurprising given the alteration of sterics imposed by the substrates at each stage of the catalytic cycle.

Computational analyses

Since the crystallographic analyses indicate that the coordinated BOPA ligand adopts an arrangement where the

phenyl rings of the ligand backbone are not coplanar, and the spectroscopic data suggest that both isomers of each complex are present in solution, we calculated the two diastereomeric forms for each of the yttrium alkyl complexes, yttrium and lanthanum bis(trimethylsilyl)amide complexes, and lanthanum complexes bearing the hydroamination substrate prior to cyclisation, as a means of understanding the structure and relative energies of the isomers. The structures of the yttrium isomers of [Y(iPr-BOPA){N(SiMe$_3$)$_2$}$_2$], **2a$_{calc}$**, are displayed in Fig. 4, viewed along the BOPA–N$_{amide}$–Y bond (top) showing the helical twist, and the perpendicular view (bottom), showing the relative positioning of the stereodirecting groups (in this case isopropyl). The structures of all calculated complexes are analogous, differing principally in the M–N bond distances and reflecting the differing ionic radii of the metal ions.

The most significant difference between the two isomers (other than the helical twist) is the different orientation of the oxazoline stereodirecting groups, in that they are directed either in mutually opposite directions (*exo*) or closer together along the same face of the coordination sphere (*endo*). The crystal structures are consistent with the *exo* isomer, which is expected to be the more stable isomer on steric grounds. The relative enthalpies and Gibbs free energies for the two isomers, for each of the complexes **1$_{calc}$**–**3$_{calc}$** and **7$_{calc}$**, are provided in Table 4.

The relative enthalpies and Gibbs free energies of the *exo* and *endo* isomers of the yttrium alkyl complexes **1$_{calc}$** generally favour the *exo* isomer, as expected, and are consistent with this isomer being the major component in the solution state

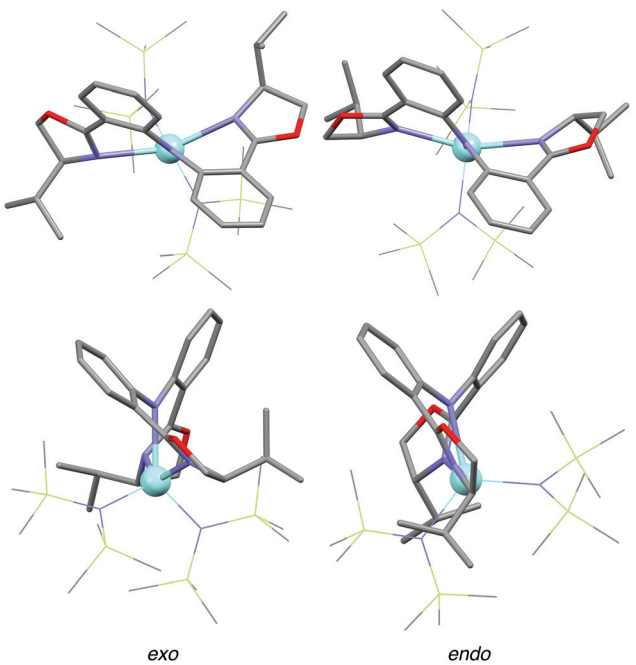

Fig. 4 Calculated structures of [Y(iPr-BOPA){N(SiMe$_3$)$_2$}$_2$] **2a$_{calc}$**. Top: view along BOPA–N$_{amide}$–Y bond; bottom: side view showing relative orientation of stereodirecting groups.

Table 4 Calculated relative enthalpies and Gibbs free energies (kcal mol^{-1}) at 298 K for the *exo* and *endo* isomers of [Ln(R-BOPA)X$_2$] **1$_{calc}$**, **2$_{calc}$**, **3$_{calc}$**, **7$_{calc}$**

Complex	R	$\Delta H_{calc.}$ ($\Delta G_{calc.}$) (*vacuo*)[a]	$\Delta H_{calc.}$ ($\Delta G_{calc.}$) (benzene)[a]
[Y(R-BOPA)(CH$_2$SiMe$_2$Ph)$_2$] **1$_{calc}$**	iPr	6.6 (5.9)	5.5 (5.4)
	Ph	1.6 (3.4)	2.1 (3.3)
	Bn	2.9 (2.2)	2.8 (2.3)
[Y(R-BOPA){N(SiMe$_3$)$_2$}$_2$] **2$_{calc}$**	iPr	−1.1 (−0.6)	−1.7 (−0.6)
	Ph	6.0 (7.0)	5.5 (6.8)
	Bn	3.3 (3.6)	3.0 (1.5)
[La(R-BOPA){N(SiMe$_3$)$_2$}$_2$] **3$_{calc}$**	iPr	0.5 (−0.1)	0.3 (1.4)
	Ph	6.1 (6.1)	5.7 (6.5)
	Bn	2.1 (2.3)	1.3 (1.0)
[La(R-BOPA)(NHCH$_2$CPh$_2$C$_3$H$_5$)$_2$] **7$_{calc}$**	iPr	2.6 (2.6)	2.7 (4.4)
	Ph	4.9 (7.7)	4.9 (5.9)
	Bn	2.8 (2.7)	3.0 (4.4)

[a] $G_{calc.}$(*endo*) − $G_{calc.}$(*exo*).

studies (*vide supra*). These calculations suggest that, experimentally, the isopropyl congener **1a** should show the greatest level of preference for the *exo* isomer, followed by the phenyl and benzyl derivatives **1b** and **1c** respectively, which is contrary to the data obtained from the NMR spectra; calculating the relative energies in the presence of a solvent field leaves the energies largely unaffected. An analysis of the structures indicates that there is a significant flexibility in the alkyl co-ligand, which undergoes a substantial conformational change between the *exo* and *endo* isomers. This flexibility is likely to render the gas phase calculations more ambiguous, and consequently less representative of the solution state measurements. Moreover, and adding a solvent field to the calculations does not take due consideration of discrete solvent–substrate interactions (*e.g.* π stacking interactions). These limitations notwithstanding, the calculations clearly indicate that both isomers are energetically accessible, and therefore expected to be implicated in a detailed analysis of their coordination chemistry. Such a conclusion is entirely consistent with the experimental observations discussed above.

The yttrium and lanthanum bis(trimethylsilyl)amido complexes **2$_{calc}$** and **3$_{calc}$** possess more rigid co-ligands than their alkyl counterparts, and therefore the steric interactions between the stereodirecting groups and the co-ligands is likely to have a greater influence on the relative energies of the two isomers, exhibiting a stronger correlation with the size and rigidity of the stereodirecting group. In each case, the energies lie in the order iPr < Bn < Ph. The relative ordering of the isopropyl and phenyl groups is unsurprising, since phenyl groups have a significantly larger steric footprint than isopropyl groups. The positioning of the benzyl group is less obvious at first sight, and we attribute this to the higher level of flexibility offered to a benzyl group in virtue of possessing a methylene group between the oxazoline ring and the phenyl group. This interpretation is supported by the luminescence studies of the

neodymium complexes **5a–c**, in which the relative proportion of the *endo* isomer is found in the order iPr > Bn > Ph. The ordering of the relative energies for the lanthanum complexes mirrors those of the yttrium complexes for each of the stereodirecting groups. However, the energies for the yttrium complexes are universally higher than for lanthanum. Although the energy differences are relatively small (with respect to the accuracy of computational methods) we suggest that this trend arises as a result of the ionic radius of the metal ion which, being smaller for yttrium, results in greater steric repulsion as a result of shorter interatomic distances between the lanthanide and the coordinating nitrogens.

Upon incorporating the *pseudo*-substrate, the relative energies of the *exo* and *endo* isomers of [La(R-BOPA)-$(NHCH_2CPh_2C_3H_5)_2$] **7$_{calc}$** change significantly in the relative ordering. The complex bearing the phenyl stereodirecting group remains the derivative that most favours the *exo* isomer, whilst the isopropyl and benzyl congeners are essentially identical in their respective values for $\Delta H_{calc.}$ and $\Delta G_{calc.}$. The relative ordering of these values is unchanged when a solvent field is introduced. In an analogous manner to the discussion of the alkyl complexes, these energies less reliably reproduce the experimental proportions, which again is likely to arise from the significant flexibility of the co-ligand and therefore the possible conformations that exist in solution, compared to the gas phase calculations. Nevertheless, these calculated structures (Fig. 5) show that with such flexible co-ligands, the accessibility of the metal is substantially different for the *exo* and *endo* isomers. This observation explains the relative lifetimes observed for the two isomers in the luminescence studies, since the *endo* isomer contains a more solvent-accessible metal centre and should be more easily quenched by solvent molecules (*i.e.* should have a shorter radiative lifetime, as observed experimentally). These calculated structures also provide insight into the stereocontrol offered by the two conformations in catalytic reactions. Given the manner in which the tethered amidoalkene inserts into the M–N bond, it is likely that the *exo* isomer exerts a greater degree of stereocontrol over the catalytic reaction during the stereodirecting insertion step, compared to the *endo* isomer, since the stereodirecting groups effectively shield a greater proportion of the accessible coordination sphere in the *exo* isomer. We therefore propose that the presence of two species with potentially different stereodirecting ability is likely to have a significant impact on the complexes' overall ability to invoke stereocontrol in the catalysis.

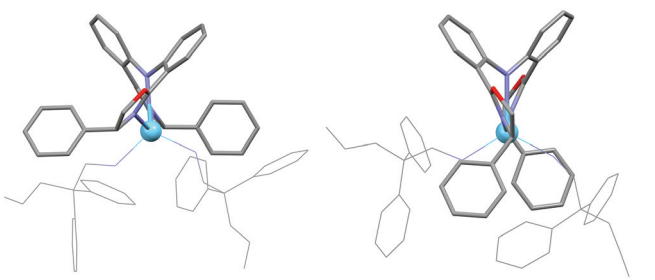

Fig. 5 *Exo* (left) and *endo* (right) isomers of [La(R-BOPA)-$(NHCH_2CPh_2C_3H_5)_2$].

Catalytic applications of lanthanide BOPA complexes

The catalytic applications of lanthanide complexes have been subject to sustained interest over a number of years. The complexes employed in such processes have been diverse, and complexes bearing oxazoline-containing ligands are no exception.[1j] However, owing to the relative underrepresentation of organometallic and related complexes bearing chiral oxazoline ligands, it is appropriate to probe the efficacy of these lanthanide BOPA complexes in catalytic reactions typical of this class of complex, namely the intramolecular hydroamination/cyclisation of aminoalkenes, and the ring-opening polymerisation of *rac*-lactide.

Hydroamination/cyclisation of aminoalkenes

Whilst there have been remarkable developments in the catalytic applications of lanthanide complexes supported by oxazoline-based ligands, particularly in Lewis acid catalysis, their application in hydroamination catalysis has been relatively limited.[1j] In 2003 Marks *et al.* showed that lanthanide complexes bearing the bis(oxazolinyl)methane (BOX) ligand were active towards the intramolecular hydroamination/cyclisation of aminoalkenes, forming chiral heterocycles in up to 67% ee.[15a] For many reactions catalysed by lanthanide-oxazoline complexes, the incorporation of an additional donor between the oxazoline moieties has afforded catalysts with much improved reactivity and selectivity, as observed in the neutral pyridine-bis(oxazoline) ligand, PYBOX.[31] Accordingly it was of interest to probe the efficacy of Group 3/lanthanide complexes bearing the chiral BOPA ligand in the intramolecular hydroamination reaction.

Complexes **1–6** were employed in the intramolecular hydroamination of aminoalkenes **A** and **B**, bearing geminal methyl and phenyl substituents respectively (Scheme 4). Selected catalytic data are provided in Table 5, whilst a complete list of performance data is provided in the ESI.† The yttrium amides **2** were unreactive under a variety of conditions, including at elevated temperatures. In contrast, the alkyl complexes **1a–c** were active and gave good conversions within 15 min. at room temperature for substrate **B**. Given that the active species in this case, once the alkyl ligands have been replaced by tethered amido-alkenes, is identical regardless of the identity of the initial co-ligand,[32] this suggests that the yttrium amide complexes **2** do not enter the catalytic cycle, possibly as a result of the steric demands of the bulky bis(trimethylsilyl)amide co-

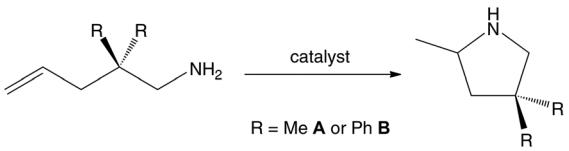

Scheme 4 Intramolecular hydroamination of aminoalkenes.

Table 5 Intramolecular hydroamination of aminoalkenes by [Y(R-BOPA)($CH_2SiMe_2Ph)_2$] or [Ln(R-BOPA){$N(SiMe_3)_2$}$_2$][a]

Entry	Ln	Catalyst	R	Substrate	Temp./°C	% Conv.	Time[b]	Solvent	ee[c]
1	Y	**1a**	iPr	**B**	22	>99	15 min	C_6D_6	43
2		**1b**	Ph	**B**	22	>99	15 min	C_6D_6	−44[d]
3		**1c**	Bn	**B**	22	>99	15 min	C_6D_6	30
4		**1a**	iPr	**B**	22	>99	12 h	Tol-D_8	40
5		**1b**	Ph	**B**	22	>99	12 h	Tol-D_8	−42
6		**1c**	Bn	**B**	22	>99	12 h	Tol-D_8	26
7		**10a**	iPr	**B**	22	>99	15 min	C_6D_5Br	38
8		**10b**	Ph	**B**	22	>99	15 min	C_6D_5Br	−36
9		**10c**	Bn	**B**	22	>99	15 min	C_6D_5Br	32
10	La	**3a**	iPr	**A**	30	>99	72 h	C_6D_6	7
11		**3b**	Ph	**A**	30	>99	72 h	C_6D_6	−28
12		**3c**	Bn	**A**	30	>99	72 h	C_6D_6	6
13		**3a**	iPr	**B**	22	>99	15 min	C_6D_6	5
14		**3b**	Ph	**B**	22	>99	15 min	C_6D_6	−25
15		**3c**	Bn	**B**	22	>99	15 min	C_6D_6	6
16		**3a**	iPr	**B**	22	>99	12 h	Tol-D_8	6
17		**3b**	Ph	**B**	22	>99	12 h	Tol-D_8	−45
18		**3c**	Bn	**B**	22	>99	12 h	Tol-D_8	6
19	Pr	**4a**	iPr	**B**	22	>99	1 h	C_6D_6	16
20		**4b**	Ph	**B**	22	>99	1 h	C_6D_6	−18
21		**4c**	Bn	**B**	22	>99	1 h	C_6D_6	42
22		**4a**	iPr	**A**	22	>99	12 h	C_6D_6	14
23		**4b**	Ph	**A**	22	>99	12 h	C_6D_6	−16
24		**4c**	Bn	**A**	22	>99	12 h	C_6D_6	10
25		**4a**	iPr	**B**	22	>99	12 h	Tol-D_8	18
26		**4b**	Ph	**B**	22	>99	12 h	Tol-D_8	−26
27		**4c**	Bn	**B**	22	>99	12 h	Tol-D_8	4
28	Nd	**5a**	iPr	**B**	22	>99	<15 min	C_6D_6	12
29		**5b**	Ph	**B**	22	>99	<15 min	C_6D_6	−24
30		**5c**	Bn	**B**	22	>99	<15 min	C_6D_6	10
31		**5a**	iPr	**A**	22	—	1 week	C_6D_6	—
32		**5b**	Ph	**A**	22	<10	1 week	C_6D_6	−14
33		**5c**	Bn	**A**	22	—	1 week	C_6D_6	—
34		**5a**	iPr	**B**	22	>99	12 h	Tol-D_8	36
35		**5b**	Ph	**B**	22	>99	12 h	Tol-D_8	−44
36		**5c**	Bn	**B**	22	>99	12 h	Tol-D_8	46
37	Sm	**6a**	iPr	**B**	22	>99	1 h	C_6D_6	20
38		**6b**	Ph	**B**	22	>99	1 h	C_6D_6	−16
39		**6c**	Bn	**B**	22	>99	1 h	C_6D_6	28
40		**6a**	iPr	**A**	22	>99	12 h	C_6D_6	14
41		**6b**	Ph	**A**	22	>99	12 h	C_6D_6	−16
42		**6c**	Bn	**A**	22	>99	12 h	C_6D_6	12
43		**6a**	iPr	**B**	22	>99	12 h	Tol-D_8	30
44		**6b**	Ph	**B**	22	>99	12 h	Tol-D_8	−28
45		**6c**	Bn	**B**	22	>99	12 h	Tol-D_8	30

[a] Conditions: 10 mol% precatalyst, 0.5 mL solvent. [b] Determined from ^{1}H NMR spectra when no further conversion observed. [c] Determined by ^{1}H NMR using *R*-(−)-*O*-acetylmandelic acid. [d] The enantiomeric excesses obtained using the phenyl catalysts favoured the opposite stereochemistry owing to the opposite absolute configuration of the oxazoline groups.

ligands, consistent with the forcing conditions required for the reaction of the BOPA protio-ligand with Y{$N(SiMe_3)_2$}$_3$. The cyclisation of the geminal dimethyl substrate **A** using **1** was unsuccessful, even under forcing conditions. It is a common observation that intramolecular hydroamination/cyclisation is often highly substrate specific, both in terms of selectivity and reaction rate, and previous reports have stated that **B** is invariably cyclised more readily than **A** under otherwise identical conditions.[33] Substrate **B** was cyclised with moderate enantioselectivity with the benzyl derivative **1c** giving the lowest enantiomeric excesses. The selectivity showed no significant dependence on the temperature or solvent, although the reactions were significantly slower when performed in toluene instead of benzene.

Since sterics appear to play an important role in the effectiveness of the hydroamination catalysis, one of the alkyl co-ligands was removed by preparing the cationic complexes [Y(R-BOPA)(CH_2SiMe_2Ph)][$B(C_6F_5)_4$] (R = iPr **10a**, Ph **10b**, Bn **10c**) from the dialkyl complexes **1** and trityl perfluorophenylborate in bromobenzene-D_5 (Scheme 5). Owing to the well-documented instability of such complexes,[34] they were prepared and reacted *in situ*. Analysis by NMR spectroscopy indicated the quantitative conversion to the cationic species illustrated in Scheme 5, alongside signals attributed to $Ph_3CCH_2SiMe_2Ph$. As for their parent complexes, **10a–c** were found to be active in the cyclisation of substrate **B**, but failed to catalyse the cyclisation of substrate **A**. A slight reduction in stereoselectivity was observed for all catalyst derivatives.

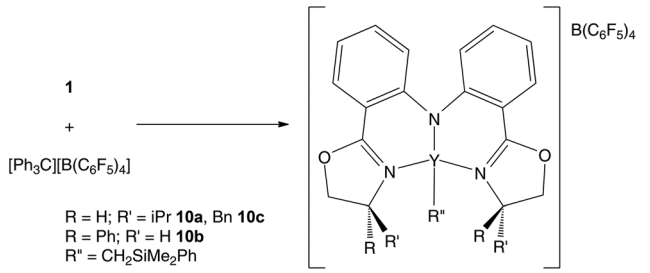

Scheme 5 *In situ* synthesis of [Y(R-BOPA)(CH_2SiMe_2Ph)][$B(C_6F_5)_4$] **10a–c**.

Given the low reactivity of substrate **A** with the yttrium complexes, we turned our attention to the larger lanthanides, employing complexes **3–6** under comparable conditions. The enantioselectivities of **3–6** are generally lower than for **1** and **10**, and is consistent with metals with larger ionic radii having the potential for larger coordination numbers, therefore giving less stereochemical preference to the substrate. In most cases complexes supported by the Ph-BOPA provided the highest levels of enantioselectivity. Although a slightly elevated temperature (30 °C) was required, substrate **A** was nevertheless cyclised successfully, albeit rather slowly and with low enantiomeric excesses (up to 28%).

Interestingly, when the cyclisations of **B** were performed in toluene instead of benzene, the room temperature selectivities, obtained with the complexes bearing Ph-BOPA, showed a significant increase from 25 to 45% ee (**3b**), 18 to 26% ee (**4b**), 24 to 44% ee (**5b**) and 16 to 28% ee (**6b**) under otherwise identical conditions. This behaviour was not observed for the yttrium catalyst **1b** (44% ee in benzene, 42% ee in toluene), neither was any enhancement observed when the catalysis was carried out in either bromobenzene or dichloromethane. An enantioselectivity dependence on the solvent is not an unknown phenomenon (although the distinction between benzene and toluene renders these results surprising) and highlights the subtle interplay of molecular conformations at the molecular level during a catalytic cycle that is, by definition, beyond exhaustive spectroscopic analysis. In the BOPA complexes described herein, we suggest that the relative energies of the *exo* and *endo* isomers, and hence the equilibrium position, can be dependent on subtle factors, such as solvent interactions and the nature/conformation of the co-ligand, and could change with each stage of a catalytic cycle. The concept of the *exo*/*endo* equilibrium position being a factor in the stereodirecting ability of the catalyst is therefore consistent with this observation, and suggests that gas phase calculations of relative energies should be treated with a degree of caution.

There is a general trend of greater enantioselectivity being obtained with the phenyl catalyst derivatives. This has often been observed with oxazoline ligands,[3,6] and can be explained in part by the fact that phenyl stereodirecting groups are often found to offer greater control over the reaction space in catalytically active complexes bearing oxazoline ligands.[3–7] However, these studies suggest an additional component to this phenomenon: the computational analyses discussed above suggest that the *exo* isomer is likely to lead to a greater degree of stereoinduction in the reaction products, compared to the *endo* isomer. The presence of these two rapidly interchanging isomers is therefore likely to have an impact on the overall catalysis performance, although in order to probe this quantitatively the stereodirecting ability and kinetics of each component would need to be measured, in accordance with a consideration of the Curtin–Hammett conditions. Unfortunately, these complexes do not lend themselves to deconvoluting the individual components of the catalysis, and it would therefore be inappropriate to directly correlate equilibrium position with catalyst performance.

Ring opening polymerisation catalysis

The ring-opening polymerisation (ROP) of cyclic esters such as ε-caprolactone (ε-CL), β-butyrolactone (BBL) and lactide (LA) to give biocompatible and/or biodegradable polymers is a topic of continuing interest, both from a materials chemistry perspective as well as a molecular catalysis standpoint.[35] Moreover, polylactides (PLAs) are United States FDA-approved for medical use. A number of synthetic methods for preparing polyesters *via* the ROP of cyclic monomers are known.[36] These are based on cationic, anionic, coordination–insertion, activated monomer, enzymatic and organocatalytic mechanisms. With respect to the work described herein, the most relevant type of initiators are coordination complexes of the type (L)M–X which initiate and propagate the ROP of lactide through the coordination–insertion mechanism as illustrated in Scheme 6 for the case of *rac*-LA. As summarised in several recent reviews,[36k–r] the identity of the supporting ligands "L" as well as the specific metal and the initiating group M–X, have a profound influence on the resultant polymer molecular weight and molecular weight distribution, and tacticity (in the case of LA for example). These in turn are the critical parameters that control the macroscopic properties of the polymers formed.

Some of the most active ROP initiators reported to date for the synthesis of PLA, the polymer of interest to us in this contribution, are based on the Group 3 and lanthanide metals.[36j,n,p,q] In addition to activity, control of the PLA product tacticity

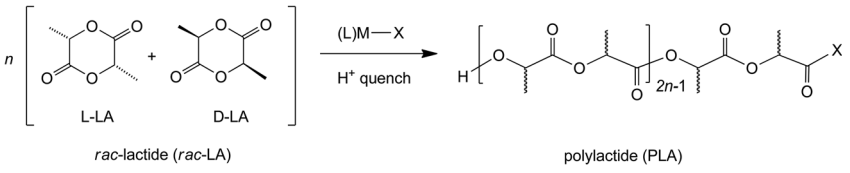

Scheme 6 ROP of *rac*-LA by the coordination–insertion mechanism.

(*e.g.* heterotactic, isotactic, stereoblock in the case of *rac*-LA) is a key parameter of interest.[36t] Most coordination complex ROP initiators are based on non-chiral metal complexes. Nonetheless, in a number of instances, non-random polymer tacticity is observed and occurs through a chain-end control mechanism.[36p,q,37] In addition, a number of complexes have also been reported which attempt to use chirality at metal (or in the ligand periphery) to achieve tacticity control, based on enantiomorphic site effects, and in a number of cases considerable control over the polymer microstructure has been achieved.[38]

Interestingly, although oxazoline-based ligands have been used extensively in catalysis in general, their use to date in cyclic ester ring-opening[11,39] or olefin[8–10,12,17,40] polymerisation catalysis is very limited indeed. In the context of ROP, in 2006, Carpentier *et al.* evaluated chiral and achiral yttrium and lanthanum bis(oxazoline) complexes for the polymerisation of *rac*-LA and *rac*-BBL.[11] Although these were found to be highly active, reaching 98% conversion after 5 min and forming polymers with narrow polydispersities (M_w/M_n) of 1.07 to 1.44, no stereoselectivity was observed. More recently, Chen *et al.* have reported a series of amido-mono(oxazoline) complexes of main group metals and zinc, but only for the ROP of L-LA (and hence the question of stereocontrol is effectively redundant in these studies).[39a–d] We were therefore interested to explore the potential of selected BOPA complexes for the ROP of *rac*-LA.

Table 6 summarises our results for the ROP of *rac*-LA with [M(R-BOPA)X_2] (M = Y (**1** or **2**), Sm (**6**) or La (**3**); R = iPr (**a**), Ph (**b**) or Bn (**c**); X = CH_2SiMe_2Ph or $N(SiMe_3)_2$) which allow the systematic evaluation of the effects of the BOPA R-substituent, metal covalent radius (Y < Sm < La) and initiating group (alkyl *vs.* amide). Polymerisation experiments were performed in THF at 25 °C with a [*rac*-LA]$_0$: [initiator] ratio of 100 : 1, and under these conditions all complexes were found to be active. The progress of each run was monitored by regular sampling (^{1}H NMR measurement of % *rac*-LA conversion to PLA) and the molecular weights and polydispersity indices (PDIs, M_w/M_n) were determined by GPC using the appropriate Mark–Houwink corrections.[41] P_r values (probabilities of racemic enchainment) were determined from the selectively homonuclear decoupled ^{1}H NMR spectra of the polymers.[42] Standard kinetic analyses were used to determine the apparent rate constant (k_{app}) for lactide consumption, and in almost all cases there was a second order dependence on [*rac*-LA] which is unusual, but not unprecedented.[37f,h,43,44] Fig. 6 shows plots of % conversion *vs.* time, M_n and PDI *vs.* % conversion, and a kinetic plot for [Y(Ph-BOPA){N($SiMe_3$)$_2$}$_2$] (**2b**) as a representative example of the amide systems. Corresponding data for all the other compounds tested are provided in the ESI (Figs. S5.1–S5.11†).

In general terms, as has been reported for other metal alkyl or amide initiators,[37a,e,45] the experimental number average molecular weights (M_n(GPC)) were considerably higher (especially in the case of the alkyl species **1a–c**) than predicted based on % conversion and one (M_n(calcd)) or two (*i.e.* approximately half the values given for M_n(calcd) in Table 6) PLA chains growing per metal centre. Entries 1–6 in Table 6 show that the PDI values for the PLAs formed are moderate for the dialkyl complexes **1a–c** (*ca.* 1.2–1.4 (but molecular weight control is much worse)) but somewhat broader (*ca.* 1.4–2.0 for most cases) with the amide counterparts (entries 7–18). These values are consistent with the poor initiator ability of alkyls and amides in general and the various transesterification side-

Table 6 ROP of rac-LA with M(R-BOPA)X_2 (M = Y (**1**), Sm (**6**) or La (**3**); R = iPr (**a**), Ph (**b**) or Bn (**c**); X = CH_2SiMe_2Ph or $N(SiMe_3)_2$)[a]

Entry	Initiator	% Conversion[b]	Time (min)	k_{app}[c]	M_n (GPC)[d]	M_n (calcd)[e]	M_w/M_n	P_r[f]
1	[Y(iPr-BOPA)(CH_2SiMe_2Ph)$_2$] (**1a**)	95	0.5	[g]	32 000	13 805	1.18	0.72
2	[Y(iPr-BOPA)(CH_2SiMe_2Ph)$_2$] (**1a**)	99	1.5	[g]	30 080	14 357	1.24	0.73
3	[Y(Ph-BOPA)(CH_2SiMe_2Ph)$_2$] (**1b**)	73	0.5	[g]	30 740	10 726	1.24	0.78
4	[Y(Ph-BOPA)(CH_2SiMe_2Ph)$_2$] (**1b**)	95	1.5	[g]	35 450	13 881	1.38	0.76
5	[Y(Bn-BOPA)(CH_2SiMe_2Ph)$_2$] (**1c**)	78	0.5	[g]	23 780	11 376	1.24	0.71
6	[Y(Bn-BOPA)(CH_2SiMe_2Ph)$_2$] (**1c**)	95	1.5	[g]	31 070	13 484	1.23	0.69
7	[Y(iPr-BOPA){N($SiMe_3$)$_2$}$_2$] (**2a**)	88	300	1.52(5) M^{-1} h^{-1}	17 880	12 791	1.55	0.70
8	[Y(Ph-BOPA){N($SiMe_3$)$_2$}$_2$] (**2b**)	90	240	2.88(9) M^{-1} h^{-1}	19 590	13 133	1.36	0.71
9	[Y(Bn-BOPA){N($SiMe_3$)$_2$}$_2$] (**2c**)	81	15	—	15 720	11 840	1.54	0.81
10	[Y(Bn-BOPA){N($SiMe_3$)$_2$}$_2$] (**2c**)	98	120	16.1(7) M^{-1} h^{-1}	22 290	14 286	1.44	0.73
11	[Sm(iPr-BOPA){N($SiMe_3$)$_2$}$_2$] (**6a**)	90	300	1.90(3) M^{-1} h^{-1}	13 220	13 199	1.92	0.66
12	[Sm(Ph-BOPA){N($SiMe_3$)$_2$}$_2$] (**6b**)	87	255	1.56(2) M^{-1} h^{-1}	13 540	12 631	1.84	0.68
13	[Sm(Bn-BOPA){N($SiMe_3$)$_2$}$_2$] (**6c**)	38	30	—	35 890	5 586	1.95	0.81
14	[Sm(Bn-BOPA){N($SiMe_3$)$_2$}$_2$] (**6c**)	88	210	2.1(1) M^{-1} h^{-1}	21 400	12 779	1.54	0.77
15	[La(iPr-BOPA){N($SiMe_3$)$_2$}$_2$] (**3a**)	88	10	—	22 750	12 844	2.15	0.68
16	[La(iPr-BOPA){N($SiMe_3$)$_2$}$_2$] (**3a**)	98	60	13.4(2) h^{-1}	9 770	14 290	4.44	0.68
17	[La(Ph-BOPA){N($SiMe_3$)$_2$}$_2$] (**3b**)	90	120	11.1(2) M^{-1} h^{-1} [h]	12 570	13 076	2.29	0.68
18	[La(Bn-BOPA){N($SiMe_3$)$_2$}$_2$] (**3c**)	92	150	5.6(4) M^{-1} h^{-1}	20 690	13 259	1.43	0.72

[a] Conditions: [*rac*-LA]$_0$: [initiator] = 100 : 1, 4.0 mL THF at 25 °C, [*rac*-LA]$_o$ = 1.00 M. See Experimental section for other details. [b] Conversion determined by ^{1}H NMR for an aliquot taken at the stated time. [c] Apparent rate constant with units h^{-1} or M^{-1} h^{-1} derived from the first- or second-order log plots, respectively, over 3 half-lives, respectively (all systems were second-order with respect to *rac*-LA except for entries 11–12; see ESI for further details. [d] Molecular weights (g mol^{-1}) determined by GPC in THF at 30 °C using the appropriate Mark–Houwink corrections.[41] [e] Expected M_n (g mol^{-1}) for 1 chain growing per metal centre at the stated % conversions assuming CH_2SiMe_2Ph (entries 1–6) or $N(SiMe_3)_2$ (entries 7–18) initiating groups. [f] P_r measured at between 75%–90% conversion except for entry 13. [g] k_{app} not measured. [h] Measured in the linear region up to 80% conversion (see Fig. S3.10 of the ESI).

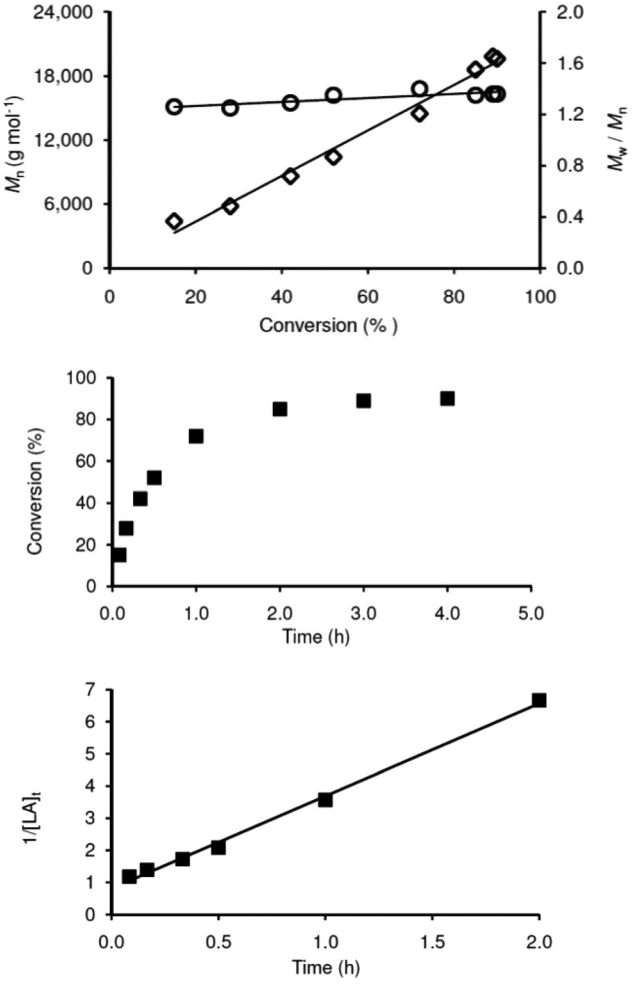

Fig. 6 Data for the ROP of *rac*-LA using [Y(Ph-BOPA){N(SiMe$_3$)$_2$}$_2$] (**2b**). Top: M_n (diamonds) and M_w/M_n (circles) *vs.* % conversion: the gradient of M_n *vs.* conversion plot is 214(10) g mol^{-1} (% conversion)$^{-1}$ (R^2 = 0.986). Middle: % conversion *vs.* time. Bottom: second order plot for *rac*-LA consumption: R^2 = 0.996, k_{app} = 2.88(9) M^{-1} h^{-1}. Conditions: [*rac*-LA]$_0$: [initiator] = 100 : 1, 4.0 mL THF at 25 °C, [*rac*-LA]$_0$ = 1.00 M.

reactions (*vide infra*) that also take place. Note that it is often found that metal-alkoxide complexes (either as isolated species or generated *in situ*) are better initiators than their alkyl or amide counterparts because of a better match of initiation and propagation rates.[36k–r] Unfortunately it was not possible to prepare the corresponding alkoxide or aryloxide analogues of the [M(R-BOPA)X$_2$] complexes. For example, addition of 2 equiv. BnOH to complex **2b** in C_6D_6 failed to generate the desired [Y(Ph-BOPA)(OBn)$_2$] complex, instead resulting in the formation of the protio-ligand and unknown side-products.

In terms of the PLAs formed with the new alkyl or amide initiators, all were heterotactically enriched as judged by their P_r values, which lie broadly in the range *ca.* 0.7–0.8. Although the P_r values for all three types of R-BOPA ligand appeared in this range, the values for the amide derivatives of the smaller metals (Y and Sm) supported by Bn-BOPA (entries 9 & 10 (for **2c**) and 13 & 14 (for **6c**)) appeared to be slightly higher than for the iPr-BOPA and Ph-BOPA homologues. For the lanthanum complexes [La(R-BOPA){N(SiMe$_3$)$_2$}$_2$] (**3a–c**) there was no significant difference in P_r between the three ligands. This is consistent with the usual observation that polymerisation control generally is poorer for the larger metals.[36k–r] Compared to most Group 3 and lanthanide initiators, P_r values of around 0.8 can be considered to be good, but not exceptional, with values in excess of 0.9–0.95 being achieved in some instances).[36p,q,37f,46] Unfortunately, in the present study, we are not able to distinguish between chain-end control and enantiomorphic site control factors.[38e] As mentioned, attempts to prepare model non-chiral R-BOPA ligands and their complexes were unsuccessful.

Attempts to record MALDI-ToF mass spectra of the PLAs formed with the dialkyl complexes **1a–c** were unsuccessful due to their very high molecular weight. Analysis of the polymers formed with the amide complexes showed linear PLA with only hydroxyl end groups, as is usually the case with silylamide initiators, presumably due to hydrolysis of the expected –C(O)N(SiMe$_3$)$_2$ termini during polymer quenching and analysis. In addition, both linear and cyclic PLA was found to be present in the MALDI-ToF mass spectra, and both types of polymer showed peak envelopes with a $\Delta(m/z)$ separation of 72, *i.e.* 1/2 of a LA moiety, (*i.e.* –OCH(Me)C(O)–). These observations are consistent with both intramolecular ("back-biting") and intermolecular transesterification side-reactions.

With respect to polymerisation rates, the yttrium dialkyl complexes **1a–c** (Table 6, entries 1–6) were considerably faster than any of the amide analogues, either for yttrium (**2a–c**) or the larger metals. While these fast rates (which were too high to be accurately determined) imply rapid initiation, the much higher than predicted M_n(GPC) values still indicate that initiation is unable to match propagation as discussed above. The heterotacticity of the PLAs formed with **1a–c** (0.69–0.78) are experimentally indistinguishable from those for **2a–c** (0.70–0.81) implying similar propagating species.

The apparent propagation rate constants (k_{app}) for the yttrium and samarium iPr-BOPA (**2a**, **6a**) and Ph-BOPA (**2b**, **6b**) diamide complexes are comparable (*ca.* 1.5–3.0 M^{-1} s^{-1}), as is that for [Sm(Bn-BOPA){N(SiMe$_3$)$_2$}$_2$] (**6c**), even though the covalent radius of yttrium (1.90 Å) is somewhat smaller than that of samarium (1.98 Å).[47] Unexpectedly, however, k_{app} for [Y(Bn-BOPA){N(SiMe$_3$)$_2$}$_2$] (**2c**, k_{app} = 16.(7) M^{-1} s^{-1}) is reproducibly almost one order of magnitude larger than **2a–b** and **6**. While this has no clear explanation, the higher k_{app} values of the lanthanum complexes **3b** and **3c** (entries 17, 18) compared to those of their samarium analogues (**6b**, **6c**) would seem to be in keeping with the larger radius of lanthanum (2.07 Å). Also unexpectedly, compared to all the other amide complexes studied, [La(iPr-BOPA){N(SiMe$_3$)$_2$}$_2$] (**3a**, entry 16) showed very clear first order k_{app} dependence on [*rac*-LA] (*cf.* Fig. S5.9 in the ESI†), leading again to a much faster polymerisation rate (98% conversion after 60 min. compared to 90–92% after 120–150 min. for **3a** and **3b**). Compound **3b** also showed slightly unusual behaviour with the second order plot of 1/[LA] *vs.* time showing a deviation from linearity after approximately

80% completion of the ROP (*cf.* Fig. S3.10 in the ESI†). The k_{app} value in Table 6, entry 17 refers to data for this linear region (between two and three half-lives).

Conclusions

Whilst alkyl- and amide-based functional lanthanide complexes bearing chiral oxazoline ligands are relatively scarce outside of the ubiquitous BOX ligand, we have demonstrated that tridentate BOPA ligands provide a useful framework for supporting complexes of this type. Moreover, luminescence spectroscopy has provided a means of detecting and studying equilibria between conformational isomers of paramagnetic lanthanide complexes, owing to the faster timescale of luminescence spectroscopy, compared to NMR spectroscopy. This in turn has provided a greater level of insight into the behaviour of these complexes in a manner that is pertinent to their catalytic performance. The catalytic applications in hydroamination/cyclisation and ring-opening polymerisation serve to demonstrate the potential of these types of ligand in a number of important catalytic processes.

Experimental

General methods and instrumentation

All manipulations of air and moisture sensitive species were performed under an atmosphere of argon or dinitrogen using standard Schlenk and glove box techniques. Solvents were dried by passing through an alumina drying column incorporated into a MBraun SPS800 solvent purification system, except in the case of tetrahydrofuran, which was dried over molten potassium for three days and distilled under argon. All solvents were degassed, saturated with argon, and stored under argon in Teflon valve ampoules prior to use. $CDCl_3$ for non-sensitive samples was passed through a column of basic alumina before being stored over 4 Å molecular sieves prior to use. Deuterated solvents for NMR spectroscopy were dried over molten potassium (benzene-d_6, toluene-d_8) for three days before being vacuum transferred, freeze pump thaw degassed and stored in a glove box. All other reagents were purchased from commercial suppliers and used as received unless otherwise stated. Metal precursors were synthesised according to published procedures.[25,48]

Air sensitive samples for NMR and luminescence spectroscopy were prepared in a glove box under a dinitrogen atmosphere using 5 mm Nolan NMR tubes equipped with J. Young Teflon valves. All other samples were prepared in Wilmad 5 mm NMR tubes. NMR spectra were recorded on Bruker Avance DPX-400, -500, -600, Varian Mercury-VX, or Unity Plus 500 NMR spectrometers. NMR spectra are quoted in ppm relative to tetramethylsilane (δ = 0 ppm) and were referenced internally relative to the residual protio-solvent (^{1}H) or solvent (^{13}C) resonances, all coupling constants are quoted in Hertz. Where appropriate, NMR assignments were confirmed by the use of two-dimensional ^{1}H–^{1}H or ^{1}H–^{13}C correlation experiments (HSQC and HMBC). Infrared spectra were prepared as KBr pellets and were recorded on a Jasco 660-Plus FTIR spectrometer. Infrared data are quoted in wavenumbers (cm^{-1}). All photophysical data were obtained on a Jobin Yvon-Horiba Fluorolog-3 spectrometer fitted with a JY TBX picosecond photodetection module. A Hamamatsu R5509-73 detector (cooled to −80 °C using a C9940 housing) was used for near-IR luminescence measurements. For the near-IR lifetimes the pulsed laser source was a Continuum Minilite Nd:YAG configured for 355 nm output, whilst for fluorescence lifetimes a 459 nm NanoLEDs (operating at 1 MHz) was utilized. All lifetime data were collected using the JY-Horiba FluoroHub single photon counting module in multi-channel scalar mode. Lifetimes were obtained using the provided software, DAS6. Elemental analyses were recorded by Mr Stephen Boyer at London Metropolitan University. Full experimental procedures and characterising data for all ligand precursors and complexes are provided in the ESI.†

MALDI-ToF-MS analysis was performed on a Waters MALDI micro equipped with a 337 nm nitrogen laser. An accelerating voltage of 25 kV was applied. The polymer samples were dissolved in THF at a concentration of 1 mg mL^{-1}. The cationisation agent used was potassium trifluoroacetate (Fluka, >99%) dissolved in THF at a concentration of 5 mg mL^{-1}. The matrix used was *trans*-2-[3-(4-*tert*-butylphenyl)-2-methyl-2-propenylidene]malononitrile (DCTB) (Fluka) and was dissolved in THF at a concentration of 40 mg mL^{-1}. Solutions of matrix, salt and polymer were mixed in a volume ratio of 4 : 1 : 4, respectively. The mixed solution was hand-spotted on a stainless steel MALDI target and left to dry. The spectra were recorded in reflectron mode.

Polymer molecular weights (M_n, M_w) were determined by GPC using a Polymer Laboratories Plgel Mixed-D column (300 mm length, 7.5 mm diameter) and a Polymer Laboratories PL-GPC50 Plus instrument equipped with a refractive index detector. THF (HPLC grade) was used as an eluent at 30 °C with a flow rate of 1 mL min^{-1}. Linear polystyrenes were used as primary calibration standards, and Mark–Houwink corrections for PLA in THF were applied for the experimental samples.[41]

General procedure for hydroamination catalysis. 2,2-Diphenyl-1-amino-pent-4-ene and 2,2-dimethyl-1-amino-pent-4-ene were prepared according to literature methods.[15b] In a dinitrogen filled glovebox, the appropriate aminoalkene (0.5 mmol) was added to a solution of the corresponding pre-catalyst complex (0.05 mmol) in C_6D_6 (0.7 mL). The solution was transferred to a J. Young Teflon valve equipped NMR tube and sealed. All catalyst reactions were monitored *via* ^{1}H NMR spectroscopy periodically to monitor conversion. Upon completion, the reaction mixture was passed through silica to remove the metal residues, and a solution of (*R*)-(−)-*O*-acetylmandelic acid (0.51 mmol) predissolved in a minimal amount of $CDCl_3$ was added, producing the diastereomeric salts. The resulting enantiomeric excesses (ee) were then determined by integration of the ^{1}H NMR spectra (methyl resonance) after fitting the signals using the iNMR software program.[49]

General procedure for the polymerisation of *rac*-LA. *rac*-LA (4.00 mmol) was added to a solution of initiator (0.04 mmol) in THF (4 mL). 0.1 mL aliquots were drawn periodically and quenched with wet THF (5 mL). Volatiles were removed under reduced pressure to leave behind the polymer residue. Samples were analysed by GPC, MALDI-ToF MS and ^{1}H NMR ($CDCl_3$) spectroscopy.

Crystallographic studies

Single crystals of [Ln(Ph-BOPA){N(SiMe$_3$)$_2$}$_2$] (Ln = Nd **5b** and Sm **6b**) suitable for X-ray analysis were grown from a saturated solution in hexanes. X-ray data were collected on a Rigaku Saturn 724+ CCD diffractometer at 100 K, by the EPSRC National Crystallographic Service. The structures were solved using direct methods with absorption corrections being applied as part of the data reduction scaling procedure. After refinement of the heavy atoms, difference Fourier maps revealed the maxima of residual electron density close to the positions expected for the hydrogen atoms; they were introduced as fixed contributors in the structure factor calculations and treated with a riding model, with isotropic temperature factors (U_{iso}(H) = 1.3$U_{eq.}$(C)) but not refined. Full least-square refinement was carried out on F^2. A final difference map revealed no significant maxima of residual electron density. Structure solution and refinement were performed using the SHELX software suite.[50] Crystal data and experimental details are provided in Table S3.1.†

Density functional calculations

All calculations were performed on the Gaussian 09 program.[51] Molecular geometries were optimized without restraints, and were followed by frequency calculations to ascertain the nature of the stationary point (minimum *vs.* saddle point). Calculations were performed using the restricted B3LYP hybrid functional, with the Stuttgart/Dresden basis set with pseudo core potentials for the Y and La, 6-31G-(d,p) for all coordinating atoms, and 6-31G for all remaining centres. Coordinates of all optimised structures are provided in the ESI.†

Acknowledgements

We thank Cardiff University (Endowment Fellowship to SDB) and the Leverhulme Trust (F/00 407/BL) for financial support, and the EPSRC for access to the National Crystallographic Service[52] and studentships to BC and MPB. Access to the Advanced Research Computing Service at Cardiff University "ARCCA" is gratefully acknowledged.

References

1 For selected reviews see: (*a*) F. T. Edelmann, D. M. M. Freckmann and H. Schumann, *Chem. Rev.*, 2002, **102**, 1851; (*b*) Z. Hou and Y. Wakatsuki, *Coord. Chem. Rev.*, 2002, **231**, 1; (*c*) S. Hong and T. J. Marks, *Acc. Chem. Res.*, 2004, **37**, 673; (*d*) S. Arndt and J. Okuda, *Adv. Synth. Catal.*, 2005, **347**, 339; (*e*) G. A. Molander and J. A. C. Romero, *Chem. Rev.*, 2002, **102**, 2161; (*f*) P. M. Zeimentz, S. Arndt, B. R. Elvidge and J. Okuda, *Chem. Rev.*, 2006, **106**, 2404; (*g*) G. Zi, *Dalton Trans.*, 2009, 9101; (*h*) M. Zimmermann and R. Anwander, *Chem. Rev.*, 2010, **110**, 6194; (*i*) F. T. Edelmann, *Coord. Chem. Rev.*, 2011, **255**, 1834; (*j*) B. D. Ward and L. H. Gade, *Chem. Commun.*, 2012, **48**, 10587.

2 For selected reviews see: (*a*) J.-C. G. Bünzli, A.-S. Chauvin, H. K. Kim, E. Dieters and S. V. Eliseeva, *Coord. Chem. Rev.*, 2010, **254**, 2623; (*b*) J.-C. G. Bünzli and S. V. Eliseeva, *Chem. Sci.*, 2013, **4**, 1939; (*c*) E. G. Moore, A. P. S. Samuel and K. N. Raymond, *Acc. Chem. Res.*, 2009, **42**, 542; (*d*) F. Artizzu, M. L. Mercuri, A. Serpe and P. Deplano, *Coord. Chem. Rev.*, 2011, **255**, 2514; (*e*) P. A. Tanner and C.-K. Duan, *Coord. Chem. Rev.*, 2010, **254**, 3026; (*f*) A. D'Aléo, F. Pointillart, L. Ouahab, C. Andraud and O. Maury, *Coord. Chem. Rev.*, 2012, **256**, 1604; (*g*) X. Zhu, W.-K. Wong, W.-Y. Wong and X. Yang, *Eur. J. Inorg. Chem.*, 2011, 4651.

3 H. A. McManus and P. J. Guiry, *Chem. Rev.*, 2004, **104**, 4151.

4 G. Desimoni, G. Faita and K. A. Jorgensen, *Chem. Rev.*, 2006, **106**, 3561.

5 A. I. Meyers, *J. Org. Chem.*, 2005, **70**, 6137.

6 G. C. Hargaden and P. J. Guiry, *Chem. Rev.*, 2009, **109**, 2505.

7 A. K. Ghosh, P. Mathivanan and J. Cappiello, *Tetrahedron: Asymmetry*, 1998, **9**, 1.

8 B. D. Ward, S. Bellemin-Laponnaz and L. H. Gade, *Angew. Chem., Int. Ed.*, 2005, **44**, 1668.

9 L. Lukešová, B. D. Ward, S. Bellemin-Laponnaz, H. Wadepohl and L. H. Gade, *Dalton Trans.*, 2007, 920.

10 L. Lukešová, B. D. Ward, S. Bellemin-Laponnaz, H. Wadepohl and L. H. Gade, *Organometallics*, 2007, **26**, 4652.

11 A. Alaaeddine, A. Amgoun, C. M. Thoma, S. Dagorn, S. Bellemin-Laponnaz and J.-F. Carpentier, *Eur. J. Inorg. Chem.*, 2006, 3652.

12 B. D. Ward, L. Lukešová, H. Wadepohl, S. Bellemin-Laponnaz and L. H. Gade, *Eur. J. Inorg. Chem.*, 2009, 866.

13 X. Kang, Y. Song, Y. Luo, G. Li, Z. Hou and J. Qu, *Macromolecules*, 2012, **45**, 640.

14 Y. Pan, T. Xu, G.-W. Yang, K. Jin and X.-B. Lu, *Inorg. Chem.*, 2013, **52**, 2802.

15 (*a*) S. Hong, S. Tian, M. V. Metz and T. J. Marks, *J. Am. Chem. Soc.*, 2003, **125**, 14768; (*b*) M. R. Gagnè, C. L. Stern and T. J. Marks, *J. Am. Chem. Soc.*, 1992, **114**, 275; (*c*) Y. Li and T. J. Marks, *J. Am. Chem. Soc.*, 1996, **118**, 9295; (*d*) A. Motta, G. Lanza, I. L. Fragalà and T. J. Marks, *Organometallics*, 2004, **23**, 4097; (*e*) A. L. Reznichenko, H. N. Nguyen and K. C. Hultzsch, *Angew. Chem., Int. Ed.*, 2010, **49**, 8984; (*f*) H. M. Lovick, D. K. An and T. S. Livinghouse, *Dalton Trans.*, 2011, **40**, 7697; (*g*) H. Kaneko, H. Tsurugi, T. K. Panda and K. Mashima, *Organometallics*, 2010, **29**, 3463; (*h*) Y. Zhang, W. Yao, H. Li and Y. Mu, *Organometallics*, 2012, **31**, 4670;

(*i*) P. N. O'Shaughnessy, P. D. Knight, C. Morton, K. M. Gillespie and P. Scott, *Chem. Commun.*, 2003, 1770; (*j*) P. N. O'Shaughnessy, K. M. Gillespie, P. D. Knight, I. J. Munslow and P. Scott, *Dalton Trans.*, 2004, 2251; (*k*) P. N. O'Shaughnessy and P. Scott, *Tetrahedron: Asymmetry*, 2003, **14**, 1979; (*l*) S. Tobisch, *Dalton Trans.*, 2012, **41**, 9182; (*m*) D. Riegert, J. Collin, J.-C. Daran, T. Fillebeen, E. Schulz, D. Lyubov, G. Fukin and A. Trifonov, *Eur. J. Inorg. Chem.*, 2007, 1159; (*n*) Y. Chapurina, J. Hannendouche, J. Collin, R. Guillot, E. Schulz and A. Trifonov, *Chem. Commun.*, 2010, **46**, 6918; (*o*) J. Hannendouche and E. Schulz, *Chem.–Eur. J.*, 2013, **19**, 4972.

16 S. D. Bennett, S. J. A. Pope and B. D. Ward, *Chem. Commun.*, 2013, **49**, 6072.

17 H. Liu, J. He, Z. Liu, Z. Lin, G. Du, S. Zhang and X. Li, *Macromolecules*, 2013, **46**, 3257.

18 B. D. Ward, H. Risler, K. Weitershaus, S. Bellemin-Laponnaz, H. Wadepohl and L. H. Gade, *Inorg. Chem.*, 2006, **45**, 7777.

19 H. A. McManus and P. J. Guiry, *J. Org. Chem.*, 2002, **67**, 8566.

20 S.-F. Lu, D.-M. Du, S.-W. Zhang and J. Xu, *Tetrahedron: Asymmetry*, 2004, **15**, 3433.

21 H. A. McManus, P. G. Cozzi and P. J. Guiry, *Adv. Synth. Catal.*, 2006, **348**, 551.

22 T. Inagaki, L. T. Phong, A. Furuta, J.-I. Ito and H. Nishiyama, *Chem.–Eur. J.*, 2010, **16**, 3090.

23 Y. Jia, W. Yang and D.-M. Du, *Org. Biomol. Chem.*, 2012, **10**, 4739.

24 D. J. H. Emslie, W. E. Piers and R. MacDonald, *J. Chem. Soc., Dalton Trans.*, 2002, 293.

25 D. J. H. Emslie, W. E. Piers, M. Parvez and R. McDonald, *Organometallics*, 2002, **21**, 4226.

26 D. A. Fletcher, R. F. McMeeking and D. J. Parkin, *Chem. Inf. Comput. Sci.*, 1996, **36**, 746 (The UK Chemical Database Service: CSD version 5.35 updated November 2013).

27 For selected examples of Y–H and Y–C coupling constants see: (*a*) S. Banbirra, D. van Leusen, A. Meetsma, B. Hessen and J. H. Teuben, *Chem. Commun.*, 2001, 637; (*b*) D. J. H. Emslie, W. E. Piers and R. MacDonald, *J. Chem. Soc., Dalton Trans.*, 2002, 293; (*c*) F. G. N. Cloke, B. R. Elvidge, P. B. Hitchcock and V. M. E. Lamarche, *J. Chem. Soc., Dalton Trans.*, 2002, 2413; (*d*) C. Cai, L. Toupet, C. W. Lehmann and J. Carpentier, *J. Organomet. Chem.*, 2003, **683**, 131; (*e*) C. S. Tredget, S. L. Lawrence, B. D. Ward, R. G. Howe, A. R. Cowley and P. Mountford, *Organometallics*, 2005, **24**, 3136.

28 A. Beeby and S. Faulkner, *Chem. Phys. Lett.*, 1997, **266**, 116.

29 (*a*) J.-C. G. Bünzli, A.-S. Chauvin, H. K. Kim, E. Dieters and S. V. Eliseeva, *Coord. Chem. Rev.*, 2010, **254**, 2623; (*b*) S. Faulkner, S. J. A. Pope and B. P. Burton-Pye, *Appl. Spectrosc. Rev.*, 2005, **40**, 1.

30 (*a*) W. D. Horrocks Jr. and D. R. Sudnick, *Acc. Chem. Res.*, 1981, **14**, 384; (*b*) E. G. Moore, A. P. S. Samuel and K. N. Raymond, *Acc. Chem. Res.*, 2009, **42**, 542; (*c*) A. Beeby, I. M. Clarkson, R. S. Dickins, S. Faulkner, D. Parker, L. Royle, A. S. de Sousa, J. A. G. Williams and M. Woods, *J. Chem. Soc., Perkin Trans. 2*, 1999, 493.

31 For a pertinent example in the 1,3-dipolar cycloaddition of nitrones with alkenes, see: A. I. Sanchez-Blanco, K. V. Gothelf and K. A. Jørgensen, *Tetrahedron Lett.*, 1997, **38**, 7923.

32 It is theoretically possible that only one of the co-ligands is protonated by the substrate, which would mean that the active species derived from a dialkyl complex would be different from that derived from a bis(amide) complex. In this study we do not see any evidence for this situation, and reaction of complex **2** with stoichiometric hydroamination substrate did not lead to any alteration of the NMR signals attributed to **2**, see ref. 15.

33 For recent examples comparing these substrates see: (*a*) J. S. Wixey and B. D. Ward, *Chem. Commun.*, 2011, **47**, 5449; (*b*) J. S. Wixey and B. D. Ward, *Dalton Trans.*, 2011, **40**, 7693; (*c*) T. D. Nixon and B. D. Ward, *Chem. Commun.*, 2012, **48**, 11790.

34 P. M. Zeimentz, S. Arndt, B. R. Elvidge and J. Okuda, *Chem. Rev.*, 2006, **106**, 2404.

35 (*a*) E. Chiellini and R. Solaro, *Adv. Mater.*, 1996, **8**, 305; (*b*) K. E. Uhrich, S. M. Cannizzaro, R. S. Langer and K. M. Shakesheff, *Chem. Rev.*, 1999, **99**, 3181; (*c*) Y. Ikada and H. Tsuji, *Macromol. Rapid Commun.*, 2000, **21**, 117; (*d*) R. E. Drumright, P. R. Gruber and D. E. Henton, *Adv. Mater.*, 2000, **12**, 1841; (*e*) A.-C. Albertsson and I. K. Varma, *Biomacromolecules*, 2003, **4**, 1466; (*f*) R. Auras, B. Harte and S. Selke, *Macromol. Biosci.*, 2004, **4**, 835; (*g*) C. K. Williams and M. A. Hillmyer, *Polym. Rev.*, 2008, **48**, 1; (*h*) A. P. Dove, *Chem. Commun.*, 2008, 6446; (*i*) M. Kakuta, M. Hirata and Y. Kimura, *J. Macromol. Sci., Polym. Rev.*, 2009, **49**, 107; (*j*) E. S. Place, J. H. George, C. K. Williams and M. M. Stevens, *Chem. Soc. Rev.*, 2009, **38**, 1139.

36 (*a*) H. Keul and H. Hocker, *Macromol. Rapid Commun.*, 2000, **21**, 869; (*b*) M. Okada, *Prog. Polym. Sci.*, 2002, **27**, 87; (*c*) X. Lou, C. Detrembleur and C. Jérôme, *Macromol. Rapid Commun.*, 2003, **24**, 161; (*d*) S. Penczek, M. Cypryk, A. Duda, P. Kubisa and S. Slomkowski, *Prog. Polym. Sci.*, 2007, **32**, 247; (*e*) C. K. Williams, *Chem. Soc. Rev.*, 2007, **36**, 1573; (*f*) N. E. Kamber, W. Jeong, R. M. Waymouth, R. C. Pratt, B. G. G. Lohmeijer and J. L. Hedrick, *Chem. Rev.*, 2007, **107**, 5813; (*g*) D. Bourissou, S. Moebs-Sanchez and B. Martin-Vaca, *C. R. Chim.*, 2007, **10**, 775; (*h*) A.-C. Albertsson and R. K. Srivastava, *Adv. Drug Delivery Rev.*, 2008, **60**, 1077; (*i*) C. Jérôme and P. Lecomte, *Adv. Drug Delivery Rev.*, 2008, **60**, 1056; (*j*) M. Labet and W. Thielemans, *Chem. Soc. Rev.*, 2009, **38**, 3484; (*k*) H. Yasuda and E. Ihara, *Bull. Chem. Soc. Jpn.*, 1997, **70**, 1745; (*l*) B. J. O'Keefe, M. A. Hillmyer and W. B. Tolman, *J. Chem. Soc., Dalton Trans.*, 2001, 2215; (*m*) G. W. Coates, *J. Chem. Soc., Dalton Trans.*, 2002, 467; (*n*) O. Dechy-Cabaret, B. Martin-Vaca and D. Bourissou, *Chem. Rev.*, 2004, **104**, 6147; (*o*) J. Wu, T.-L. Yu, C.-T. Chen and C.-C. Lin, *Coord. Chem. Rev.*, 2006, **250**, 602; (*p*) A. Amgoune, C. M. Thomas and J.-F. Carpentier, *Pure Appl. Chem.*, 2007,

79, 2013; (*q*) R. H. Platel, L. M. Hodgson and C. K. Williams, *Polym. Rev.*, 2008, **48**, 11; (*r*) C. A. Wheaton, P. G. Hayes and B. J. Ireland, *Dalton Trans.*, 2009, 4832; (*s*) N. Ajellal, J.-F. Carpentier, C. Guillaume, S. M. Guillaume, M. Helou, V. Poirier, Y. Sarazin and A. A. Trifonov, *Dalton Trans.*, 2010, **39**, 8363; (*t*) M. J. Stanford and A. P. Dove, *Chem. Soc. Rev.*, 2010, **39**, 486; (*u*) I. dos Santos Vieira and S. Herres-Pawlis, *Eur. J. Inorg. Chem.*, 2012, 765; (*v*) A. Sauer, A. Kapelski, C. Fliedel, S. Dagorne, M. Kol and J. Okuda, *Dalton Trans.*, 2013, **42**, 9007.

37 (*a*) B. M. Chamberlain, M. Cheng, D. R. Moore, T. M. Ovitt, E. Lobkovsky and G. W. Coates, *J. Am. Chem. Soc.*, 2001, **123**, 3229; (*b*) M. H. Chisholm, J. Gallucci and K. Phomphrai, *Chem. Commun.*, 2003, 48; (*c*) P. Hormnirun, E. L. Marshall, V. C. Gibson, A. J. P. White and D. J. Williams, *J. Am. Chem. Soc.*, 2004, **126**, 2688; (*d*) M. H. Chisholm, J. C. Gallucci and K. Phomphrai, *Inorg. Chem.*, 2004, **43**, 6717; (*e*) M. H. Chisholm, J. C. Gallucci and K. Phomphrai, *Inorg. Chem.*, 2005, **44**, 8004; (*f*) L. Clark, M. G. Cushion, H. D. Dyer, A. D. Schwarz, R. Duchateau and P. Mountford, *Chem. Commun.*, 2010, **46**, 273; (*g*) M. G. Cushion and P. Mountford, *Chem. Commun.*, 2011, **47**, 2276; (*h*) T. P. A. Cao, A. Buchard, X. F. Le Goff, A. Auffrant and C. K. Williams, *Inorg. Chem.*, 2012, **51**, 2157; (*i*) C. Bakewell, T. P. A. Cao, N. Long, X. F. Le Goff, A. Auffrant and C. K. Williams, *J. Am. Chem. Soc.*, 2012, **134**, 20577.

38 (*a*) Z. Zhong, P. J. Dijkstra and J. Feijen, *Angew. Chem., Int. Ed.*, 2002, **41**, 4510; (*b*) T. M. Ovitt and G. W. Coates, *J. Am. Chem. Soc.*, 1999, **121**, 4072; (*c*) A. Otero, J. Fernández-Baeza, A. Lara-Sánchez, C. Alonso-Moreno, I. Márquez-Segovia, L. F. Sánchez-Barba and A. M. Rodríguez, *Angew. Chem., Int. Ed.*, 2009, **48**, 2176; (*d*) T. M. Ovitt and G. W. Coates, *J. Am. Chem. Soc.*, 2002, **124**, 1316; (*e*) M. H. Chisholm, N. J. Patmore and Z. Zhou, *Chem. Commun.*, 2005, 125; (*f*) A. J. Chmura, C. J. Chuck, M. G. Davidson, M. D. Jones, M. D. Lunn, S. D. Bull and M. F. Mahon, *Angew. Chem., Int. Ed.*, 2007, **46**, 2280; (*g*) P. L. Arnold, J.-C. Buffet, R. P. Blaudeck, S. Sujecki, A. J. Blake and C. Wilson, *Angew. Chem., Int. Ed.*, 2008, **47**, 6033.

39 (*a*) C.-T. Chen, C.-Y. Chan, C.-A. Huang, M.-T. Chen and K.-F. Peng, *Dalton Trans.*, 2007, 4073; (*b*) C.-T. Chen, M.-T. Chen, H.-J. Weng, C.-A. Huang and K.-F. Peng, *Eur. J. Inorg. Chem.*, 2009, 2129; (*c*) M.-T. Chen, P.-J. Chang, C.-A. Huang, K.-F. Peng and C.-T. Chen, *Dalton Trans.*, 2009, 9068; (*d*) M.-T. Chen and C.-T. Chen, *Dalton Trans.*, 2011, 12886.

40 Y. Pan, T. Xu, G.-W. Yang, K. Jin and X.-B. Lu, *Inorg. Chem.*, 2013, **52**, 2802.

41 (*a*) A. Rudin and H. L. W. Hoegy, *J. Polym. Sci., Part A: Polym. Chem.*, 1972, **10**, 217; (*b*) I. Barakat, P. Dubois, R. Jérôme and P. Teyssié, *J. Polym. Sci., Part A: Polym. Chem.*, 1993, **31**, 505; (*c*) J. R. Dorgan, J. Janzen, D. M. Knauss, S. B. Hait, B. R. Limoges and M. H. Hutchinson, *J. Polym. Sci., Part B: Polym. Phys.*, 2005, **43**, 3100.

42 M. T. Zell, B. E. Padden, A. J. Paterick, K. A. M. Thakur, R. T. Kean, M. A. Hillmyer and E. J. Munson, *Macromolecules*, 2002, **35**, 7700.

43 M. P. Blake, A. D. Schwarz and P. Mountford, *Organometallics*, 2011, **30**, 1202.

44 (*a*) L. Clark, G. B. Deacon, C. M. Forsyth, P. C. Junk, P. Mountford, J. P. Townley and J. Wang, *Dalton Trans.*, 2013, **42**, 9294; (*b*) F. Bonnet, A. R. Cowley and P. Mountford, *Inorg. Chem.*, 2005, **44**, 9046; (*c*) P. I. Binda and E. E. Delbridge, *Dalton Trans.*, 2007, 4685.

45 (*a*) M. H. Chisholm, J. C. Gallucci and K. Phomphrai, *Inorg. Chem.*, 2002, **41**, 2785; (*b*) H. Y. Ma and J. Okuda, *Macromolecules*, 2005, **38**, 2665; (*c*) R. H. Platel, A. J. P. White and C. K. Williams, *Inorg. Chem.*, 2008, **47**, 6840; (*d*) Z. Zhang, X. Xu, W. Li, Y. Yao, Y. Zhang, Q. Shen and Y. Luo, *Inorg. Chem.*, 2009, **48**, 5715; (*e*) A. D. Schwarz, A. L. Thompson and P. Mountford, *Inorg. Chem.*, 2009, **48**, 10442; (*f*) H. D. Dyer, S. Huijser, N. Susperregui, F. Bonnet, A. D. Schwarz, R. Duchateau, L. Maron and P. Mountford, *Organometallics*, 2010, **29**, 3602; (*g*) A. D. Schwarz, Z. Chu and P. Mountford, *Organometallics*, 2010, **29**, 1246.

46 A. Amgoune, C. M. Thomas and J.-F. Carpentier, *Macromol. Rapid Commun.*, 2007, **28**, 693.

47 B. Cordero, V. Gomez, A. E. Platero-Prats, M. Reves, J. Echeverria, E. Cremades, F. Barragan and S. Alvarez, *Dalton Trans.*, 2008, 2832.

48 D. C. Bradley, J. S. Ghotra and F. A. Hart, *J. Chem. Soc., Dalton Trans.*, 1973, 1021.

49 *iNMR, version 4.3.0*, 2011, http://iNMR.net

50 G. M. Sheldrick, *Acta Crystallogr., Sect. A: Fundam. Crystallogr.*, 2008, **64**, 112.

51 M. J. Frisch, G. W. Trucks, H. B. Schlegel, G. E. Scuseria, M. A. Robb, J. R. Cheeseman, G. Scalmani, V. Barone, B. Mennucci, G. A. Petersson, H. Nakatsuji, M. Caricato, X. Li, H. P. Hratchian, A. F. Izmaylov, J. Bloino, G. Zheng, J. L. Sonnenberg, M. Hada, M. Ehara, K. Toyota, R. Fukuda, J. Hasegawa, M. Ishida, T. Nakajima, Y. Honda, O. Kitao, H. Nakai, T. Vreven, J. A. Montgomery Jr., J. E. Peralta, F. Ogliaro, M. Bearpark, J. J. Heyd, E. Brothers, K. N. Kudin, V. N. Staroverov, T. Keith, R. Kobayashi, J. Normand, K. Raghavachari, A. Rendell, J. C. Burant, S. S. Iyengar, J. Tomasi, M. Cossi, N. Rega, J. M. Millam, M. Klene, J. E. Knox, J. B. Cross, V. Bakken, C. Adamo, J. Jaramillo, R. Gomperts, R. E. Stratmann, O. Yazyev, A. J. Austin, R. Cammi, C. Pomelli, J. W. Ochterski, R. L. Martin, K. Morokuma, V. G. Zakrzewski, G. A. Voth, P. Salvador, J. J. Dannenberg, S. Dapprich, A. D. Daniels, O. Farkas, J. B. Foresman, J. V. Ortiz, J. Cioslowski and D. J. Fox, *Gaussian 09, Revision C.01*, Gaussian Inc., Wallingford, CT, 2010.

52 S. J. Coles and P. A. Gale, *Chem. Sci.*, 2012, **3**, 683.